Advances in Engineering Software 99 (2016) 1–8

Contents lists available at ScienceDirect

Advances in Engineering Software

journal homepage: www.elsevier.com/locate/advengsoft

Equivalent linear elastic-viscous model of shape memory alloy for isolated structures

Sharad Ghodke*, R.S. Jangid

Department of Civil Engineering, Indian Institute of Technology Bombay, Powai, Mumbai 400076, India

ARTICLE INFO

Article history:
Received 25 March 2016
Accepted 6 April 2016

Keywords:
Base isolation
Shape memory alloy
Equivalent linear
Vibration control
Hysteresis

ABSTRACT

In this investigation, the equivalent linear elastic-viscous model of shape memory alloy (SMA) is established for seismic analysis of base-isolated structures using system identification method. The necessary key parameters to express the hysteresis loop of SMA are austenite stiffness, transformation strength, ductility ratio, and stiffness ratio. These parameters are considered in the modeling. This model is developed based on the American Association of State Highway and Transportation Officials (AASHTO) isolation guidelines. In order to validate the proposed model, the base-isolated benchmark building is analyzed by using proposed equivalent linear SMA model as well as the different non-linear SMA models. The evaluation criteria given in the benchmark problem and time variation of top-floor absolute accelerations and base-displacements are considered for comparing the linear and nonlinear models of SMA. An excellent agreement is achieved between proposed equivalent linear SMA model and its nonlinear models. The seismic code recommends that the equivalent linear model of the nonlinear system can be used for carry out the response spectrum analysis of base-isolated structures. Furthermore, the non-linear model requires computationally more time and effort, especially for larger degrees of freedom system. The proposed model may be useful to design engineers in order to over come the disadvantage of non-linear models.

1. Introduction

Structures can be protected from the damaging effects of earthquakes by isolating them at ground level. A passive isolation system is one of the most effective and simplest representations to implement the above idea. By providing an isolation device between the superstructure and substructure, the time period of a base-isolated structure is elongated and shifted away from the energetic frequency content of an earthquake. Apart from the required flexibility, the isolation system also have an adequate energy dissipating mechanism and re-centering capacity. Further, it should be able to withstand under the action of vertical load coming from the weight of superstructure, and should provide lateral rigidity against in-service load condition, such as wind or blast or low intensity earthquake.

The isolation bearings can be broadly classified into two categories: elastomeric type and sliding type. Elastomeric bearings provide a flexible interface (rubber like material) between the structure and foundation. These bearings are also supplemented by lead core to enhance hysteretic damping and to provide lateral stiffness. Elastomeric rubber bearings (ERB) and lead rubber bearings (LRB) are the examples of this category. Sliding type isolation systems provide an interface to allow a structure to slide when the lateral load exceeds a threshold value. Friction pendulum systems (FPS) and resilient friction bearing isolators (RFBI) are the examples of this category.

Commercially available traditional isolation bearings such as ERB, LRB, FPS, RFBI etc. have some difficulty in replacing any device component after a strong seismic event. Moreover, they undergo large as well as residual deformations. Isolator displacement is the decision making parameter for the design of an isolation system. Large isolator displacement leads to failure of an isolation system, especially when it is subjected to a near fault earthquake. In order to over come these problems, American Association of State Highway and Transportation Officials (AASHTO) recommends that additional damping can be used to control the large isolator displacement. In this context, many investigations were carried out by researchers to control displacement of isolation bearings using semi-active Magnetorheological (MR) dampers [1–4]. The MR damper may partially solve the above-mentioned problem, but may not be entirely eliminated. Recently, many researchers have used SMA in the isolation systems to reduce its vulnerability against near fault

* Corresponding author.
E-mail addresses: ghodkesl@yahoo.com, ghodkesl@gmail.com (S. Ghodke), rsjangid@civil.iitb.ac.in (R.S. Jangid).

http://dx.doi.org/10.1016/j.advengsoft.2016.04.005
0965-9978/

motions [5–14]. SMA has many desirable properties such as super elasticity, durability and fatigue resistance. In addition to this, SMA has also an ability to reduce design displacement as well as re-centering capacity. Ozbulut et al. [15] have presented an excellent literature review on the super-elasticity of SMA and its applications in structural vibration control particularly in the area of seismic isolation.

Many international codes are available for designing the isolated structures by using traditional isolation bearings [16,17]. It is very crucial to predict the maximum displacement of an isolated structure for the design of an isolation system. It can be computed by a nonlinear dynamic (ND) analysis for the nonlinear isolation system. The ND analysis requires much effort and computational time for the analysis of base-isolated structures. Therefore, codes are recommended that the nonlinear model can be replaced by a equivalent linear model to carry out the equivalent linear dynamic (ELD) analysis or the response spectrum analysis. Thus, it is better to have an equivalent linear parameters of the nonlinear system to predict the approximate design displacement of the base-isolated structure.

Therefore, it is important to convert nonlinear system into linear one. The behavior of SMA wire is nonlinear. Linearization is a method to convert a nonlinear hysteresis into two analogues linear parameters such as effective stiffness and equivalent viscous damping. These two parameters can be computed from the area of the hysteresis loop. The contrast of non-linear model and its equivalent linear model were analyzed by many researchers for isolated structures [18–20]. The equivalent linear model of LRB for bridge structure was proposed by Hwang and Chiou [18]. This model was proposed based on AASHTO specifications. The results obtained from the equivalent linear model are comparable with the nonlinear one. The comparison of bi-linear model and its equivalent linear model of LRB system for a building were studied by Matsagar and Jangid [19]. The modeling of the linear system was based on the International Building Code (IBC) and the Uniform Building Code (UBC) specifications. The study shown that equivalent linear model can predict comparable response as that of bi-linear one. The above-mentioned studies were limited to the friction, and lead based bearings. The equivalent linear model of SMA was proposed by Ghodke and Jangid [20]. In their work, the comparison of nonlinear SMA model and its equivalent linear model were carried out for five storeys framed structure. The results shown that the equivalent linear model of the SMA gives the comparable seismic response.

In the present study, SMA supplemented ERB isolation device is used for the base-isolated benchmark building developed by Narasimhan et al.[21–23]. The aim of this study is to compare the seismic response of base-isolated benchmark building for different non-linear SMA models with the equivalent linear model through the mentioned evaluation criteria.

2. Outline of base isolated benchmark building

Fig. 1 (a) and (b) show plan and elevation of an eight-storied steel-braced frame of the base-isolated benchmark building. The floor plan of the building is L-shape up to the sixth floor and rectangular shape for remaining floors. The overall plan of the building is 82.4 m long and 54.3 m wide. The superstructure steel frame is mounted on a concrete base slab. The concrete base slab is monolithic with concrete beams. Drop panels are provided below each column. The SMA supplemented bearings are installed in between each drop panel and the sub-structure. The building is idealized as a three-dimensional linear elastic structure. In this study, the isolation system consists of 92 isolation devices as shown in Fig. 1(a). In the benchmark problem, these bearing locations are adopted to get equal contribution of all the isolation bearings in the response of the base-isolated building. Therefore, it is considered that the SMA does not deform beyond its maximum strain limit due to the adopted distribution. Although, SMA can sustain the larger forces beyond its maximum strain limit (hardening effect), but it is not necessary to use maximum strength of the SMA. Several assumptions are made for the structural system under consideration (i) the superstructure remains linear during seismic loading, (ii) the floors are assumed to be rigid and the masses are lumped at the center of mass of the floors, (iii) three degrees of freedom (DOF) are assumed at each floor at lumped mass location, (iv) fixed base structure consists of 24 DOF, and all modes are considered in the analysis, (v) the surrounding temperature is greater than the temperature at the manufacturing of SMA, and (vi) the inherent viscous damping of SMA is ignored.

The equations of motion are developed with the fixed-base properties used for the linear superstructure. With linear behavior of the superstructure, the equations of motion can be written as

$$[M_s]\{\ddot{U}_s\} + [K_s]\{U_s\} + [C_s]\{\dot{U}_s\} = -[M_s][r](\{\ddot{U}_g\} + \{\ddot{U}_b\}) \tag{1}$$

where $[M_s]$, $[C_s]$ and $[K_s]$ are the lumped mass, damping, and stiffness matrices of size 24 × 24 for the fixed base structure, respectively; $\{U_s\} = \{U_1, U_2, ...U_8\}^T$, $\{\dot{U}_s\}$ and $\{\ddot{U}_s\}$ are the unknown relative floor displacement, velocity, and acceleration vectors, respectively of size 24 × 1; the subscript numbers 1–8 represents the floor numbers; U_1 represent the vector of size 3 × 1 for considered three DOF at first floor level; $\{\ddot{U}_g\}$ and $\{\ddot{U}_b\}$ are the acceleration vectors of ground and base mass, respectively of size 3 × 1; and $[r]$ is the influence coefficients matrix of size 24 × 3.

The non-linear behavior of SMA is modeled using the Graesser–Cozzarelli model, and the forces in the bearings are transformed to the center of mass of the base using a rigid base-slab assumption. All the SMA supplemented isolation bearings can be modeled individually or globally by equivalent lumped elements at the center of mass of the base. The governing equation of motion for the base mass is written as

$$[r]^T[M_s][\{\ddot{U}_s\} + [r](\{\ddot{U}_g\} + \{\ddot{U}_b\})] + [m_b](\{\ddot{U}_g\} + \{\ddot{U}_b\}) + \{F_{rs}\} + \{F_{rb}\} = 0 \tag{2}$$

where $[m_b]$ is the diagonal mass matrix of the base mass of size 3 × 3; $\{F_{rs}\}$ is the vector of size 3 × 1, representing the resultant restoring forces of SMA wires, it can be linear or non-linear; $\{F_{rb}\}$ is the vector of size 3 × 1, representing the resultant restoring forces of ERBs; and $[r]^T$ represents the transpose of the influence coefficients matrix $[r]$.

3. Isolation system

The philosophy behind an SMA supplemented ERB isolation device is to control the large isolator displacement with nearly zero residual deformation, in which, the ERB provides horizontal flexibility and vertical stiffness. ERB consists of steel and rubber layers alternatively. The rubber layer provides relatively low shear stiffness in the horizontal plane. The steel shims provide high vertical stiffness which helps to control the rocking effects of the structure due to vertical vibrations caused by the earthquake. SMA is used along with the ERB due to its super-elasticity and damping capabilities which minimize the peak and residual isolator deformation. The SMA is wound along the corners of the ERB to provide hysteretic damping and also to add lateral stiffness along the direction of the seismic force (refer Fig. 1(c)). If f_{rsi} is the restoring force of SMA wire in ith isolator, then

$$f_{rs} = \sum_{i=1}^{92} f_{rsi} \tag{3}$$

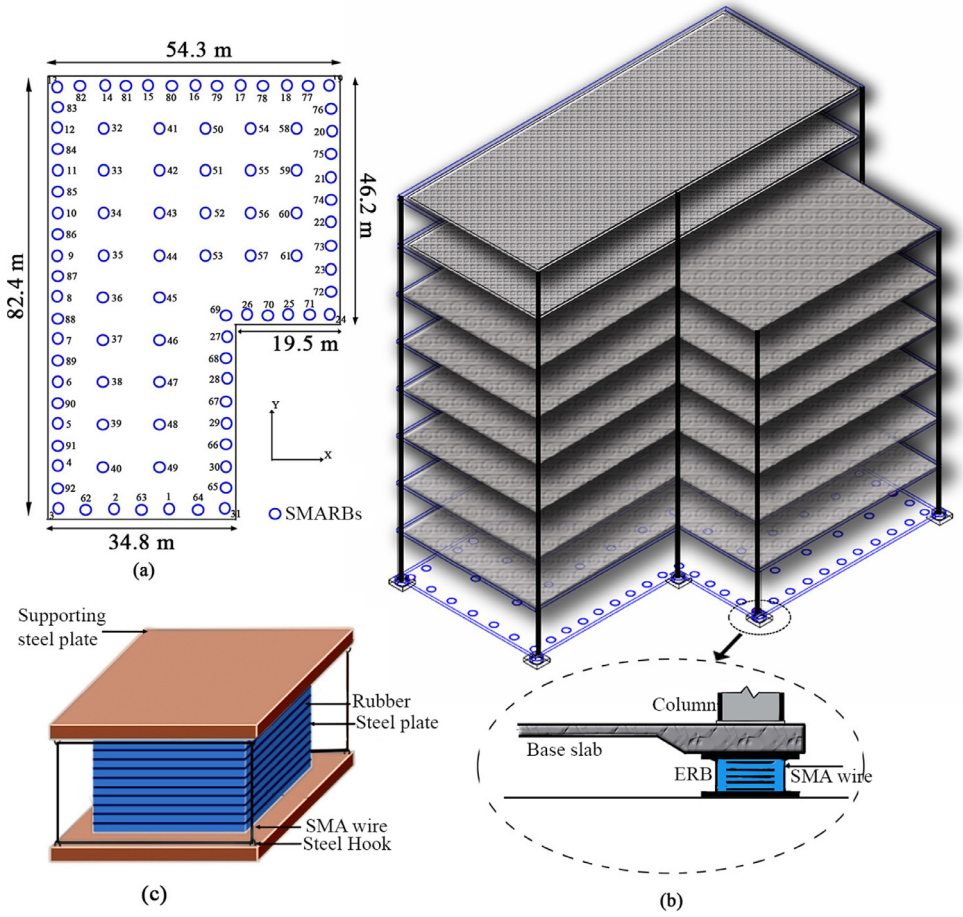

Fig. 1. (a) Plan of Base-Isolated Benchmark Building with SMA supplemented Isolation bearings. (b) Elevation of Base-Isolated Benchmark Building frame (c) SMA supplement ERB bearing (SMARB).

is the resultant restoring force of SMA wires. The resultant restoring force vector of SMA wires ($\{F_{rs}\}$) is obtained by linear or nonlinear model of SMA wire, the modeling is illustrated in Sections 3.1 and 3.2, respectively. The resultant restoring force vector of ERBs ($\{F_{rb}\}$) can be mathematically modeled as,

$$\{F_{rb}\} = [K_{rb}]\{U_b\} + [C_{rb}]\{\dot{U}_b\} \tag{4}$$

where $[K_{rb}]$ and $[C_{rb}]$ are resultant stiffness, and damping matrix of the ERBs, respectively; $\{U_b\}$ and $\{\dot{U}_b\}$ are the base displacement and velocity vectors, respectively.

If k_{bi} and k_{ti} represent the lateral stiffness of the ith ERB and SMA, respectively. Then,

$$K_b = \sum_{i=1}^{92} k_{bi} \qquad and \qquad K_t = \sum_{i=1}^{92} k_{ti} \tag{5}$$

are the resultant stiffness of the ERB and SMA devices, respectively.

The isolation period, T_b is defined as follows

$$T_b = 2\pi\sqrt{\frac{M}{K_b + K_t}} \tag{6}$$

where M is the total lumped mass of superstructure and base mass.

The damping coefficient of the ith bearing is expressed as

$$c_{bi} = 2\, m_i\, \omega_b\, \xi_b \tag{7}$$

in which, m_i is the mass of superstructure and base mass on the ith isolation device; ξ_b is damping ratio of the ERB; and ω_b is the isolation frequency defined as

$$\omega_b = \frac{2\pi}{T_b} \tag{8}$$

It is to be noted that the ω_b and T_b represents the fundamental frequency and time period of base-isolated structure if superstructure behaves rigidly. However, due to flexibility of superstructure the actual fundamental frequency and time period may slightly deviate from the above values.

3.1. Proposed equivalent linear elastic-viscous damping model of SMA

In this section an equivalent linear elastic-viscous damping model of SMA is proposed. As per the AASHTO guidelines, the nonlinear force-deformation behavior of the isolator can be replaced by an equivalent linear model [24]. This model has two parameters i.e. effective elastic stiffness and effective viscous damping. So, the linear force developed in the SMA wire can be expressed as

$$F_{SH} = K_{eff} x_b + C_{eff} \dot{x}_b \tag{9}$$

where K_{eff} and C_{eff} are the equivalent linear effective stiffness, and viscous damping, respectively.

The equivalent linear effective stiffness, and viscous damping can be obtained from area and shape of SMA hysteresis. Since, shape of the hysteresis loop has a similar pattern as that of the bi-linear hysteresis as shown in Fig. 2. Therefore, the AASHTO isolation guide specification for the bi-linear hysteretic model can be used for SMA hysteretic model to compute the equivalent effective linear stiffness of SMA.

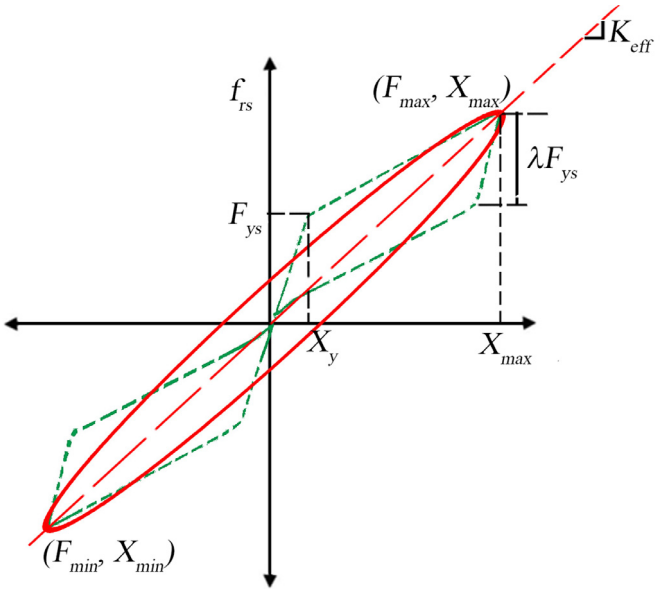

Fig. 2. SMA and its equivalent linear behavior.

- The effective stiffness can be computed from the nonlinear hysteretic loop through the expression as per AASHTO isolation guide specification

$$K_{eff} = \frac{(F_{max} - F_{min})}{(x_{max} - x_{min})} \tag{10}$$

where F_{max} and F_{min} are the forces attained for the maximum cyclic displacement x_{max} and x_{min}. Therefore, the effective stiffness of SMA is expressed as

$$K_{eff} = \frac{1 + \alpha_s(\mu - 1)}{\mu} k_a \tag{11}$$

where μ is ductility ratio of SMA defined as the design displacement under consideration (x_{max}) to yield displacement (x_y) of the SMA; and k_a is a initial austenite stiffness of SMA.

- The equivalent viscous damping expresses the effectiveness of material in the vibration damping. it is given as:

$$C_{eff} = 2\xi_{eff} M \omega_{eff} \tag{12}$$

where $\omega_{eff} = \sqrt{K_{eff}/M}$ is the effective isolation frequency; and ξ_{eff} is the effective viscous damping ratio given as

$$\xi_{eff} = \frac{W_D}{\left(2\pi K_{eff} x_{max}^2\right)} \tag{13}$$

where W_D is the energy loss per cycle from the hysteresis. The energy loss per cycle within the hysteresis is evaluated from area of hysteresis loop. The energy loss per cycle for the flag shaped hysteresis of SMA is formulated as

$$W_D = 2\lambda F_{ys}(x_{max} - x_y) \tag{14}$$

where λ F_{ys} is the shear force difference between the two transformation (during loading-unloading) of SMA as $\lambda = (1 - \alpha_s)$; α_s is the ratio of transformation stiffness to austenite stiffness of SMA.

After simplifying Eq. (12), the equivalent linear viscous damping constant is given as

$$C_{eff} = \frac{2\lambda F_{ys}(x_{max} - x_y)}{\pi \omega_{eff} x_{max}^2} \tag{15}$$

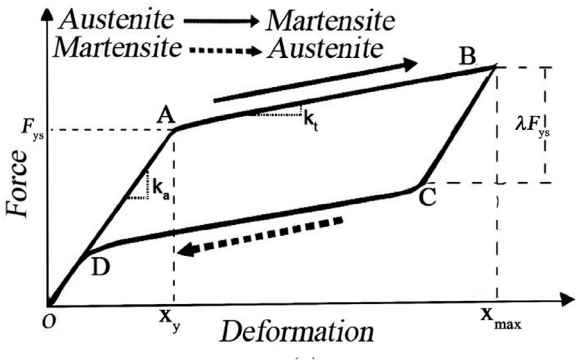

Fig. 3. Schematic load-deformation behavior of super-elastic SMA.

3.2. Nonlinear force-deformation modeling of SMA

In this section modeling of actual nonlinear force-deformation behavior of SMA wire is presented. *Super-elasticity* is one of the most important properties of SMA. *Super-elasticity*, is a recoverable response to an applied stress, caused by a phase transformation between austenite to martensite phases (refer Fig. 3). The phase transformation of SMA can be formed by applying load on it [25]. The beneficial aspect of *super-elasticity* can only be attained at elevated temperature, at which the austenite phase is stable. These are important consideration for designer because the operating temperature needs to be reasonably high to retain such effect. However, SMA manufacturer can provide required materials that can be used in the usually availed temperature ranges [15]. The present study assumes that the ambient temperature is good enough to avail such effect. In order to model *super-elasticity* of SMA, many phenomenological models have been developed by researchers ([26–30] etc.).

In this study, the classical Graesser–Cozzarelli (G-C) model and its variant are considered to model the nonlinear behavior of SMA wire. The classical G-C model is an extension of the Ozdemir's model [31]. This model is capable of providing both shape memory effect as well as the super-elastic effect. But, this model over estimates the hysteretic area (dissipated energy) within the hysteresis loop as that of an actual material [30]. Further, the hardening effect after austenite transition phase is not considered [28]. Therefore, nowadays researchers are using the G-C's extended model for their research [32–35]. However, the hardening effect is included by Wilde et al. into the classical G-C model after the austenite transition phase. This effect does not alter the effective damping and stiffness of SMA, which is of interest in the present study. Since increasing the negligible forces without increasing deformation does not affect on the dissipated energy because area within the hysteresis loop does not change. Therefore, hardening effect is neglected in this study. As the G-C model over estimates the dissipated energy of the actual material, the hysteretic area within the hysteresis loop may affect the damping of the SMA. This error can be eliminated by using improved G-C's model by Ren et al. [30]. Based on the above considered model, a MATLAB program has been coded using higher-order Runge-Kutta method to simulate the hysteretic behavior of SMA under external loading. Numerical values used for the parameters characterizing the hysteresis behavior of the SMA are provided in Table 1. The one dimensional force-deformation relationship developed by Graesser-Cozzarelli and Ren et al. are illustrated in following sections.

3.2.1. Classical Graesser–Cozzarelli model

As an extension to the Ozdemir's model, Graesser proposed one dimensional force-deformation relationship that simulates the

Table 1
Hysteresis constants for SMA and its equivalent linear model [30].

Hysteretic Parameters for G-C model	Hysteretic Parameters for Ren et al. model	Parameters for Equivalent linear model
T_b = 3 sec, n = 5, k_a = 8283 kN/m f_T = 0.08, c' = 0.001, a' = 158	k_m = 3049 kN/m n' = 3, f'_T = 1.18	x_{max} = 0.2 m, μ = 20, α_s = 0.0205 K_{eff} = 162 kN/m , β_{eff} = 0.073

super-elasticity of SMA. The equations are given as:

$$\dot{f}_{rs} = k_a\left[\dot{x}_b - |\dot{x}_b|\left(\frac{f_{rs}-\beta}{F_{ys}}\right)^n\right] \tag{16}$$

$$\beta = k_t\left\{x_b - \frac{f_{rs}}{k_a} + f_T|x_b|^{c'}erf\left(a'x_b\right)[u(-x_b\dot{x}_b]\right\} \tag{17}$$

where F_{ys} is transformation force; n is a constant controlling the sharpness of transition of hysteresis during loading changes its nature; β is the back stress; c' a constant controlling the slope of the unloading path; f_T a constant controlling the type and size of hysteresis; a' a constant controlling the amount of elastic recovery during unloading; $\dot{()}$ the ordinary time derivative; $|x_b|$ the absolute value of x_b; k_a is a initial austenite stiffness; and erf (x_b) the error function of the argument x_b,

$$erf(x_b) = \frac{2}{\sqrt{\pi}}\int_0^{x_b} e^{-t^2}dt \tag{18}$$

u() is the unit step function defined as

$$u(x) = \begin{cases} +1 & x \geq 0 \\ 0 & x < 0 \end{cases}$$

3.2.2. Extended Graesser–Cozzarelli model

As an extension to the Graesser–Cozzarelli model, Ren et al. [30] proposed one dimensional force-deformation relationship that simulates the super-elasticity of SMA. In order to simulate the force-deformation behavior of SMA more accurately, the researcher divided the full hysteresis loop in three parts: the loading path (OAB), the unloading path (BCD) up to the back transformation complete, and the elastic unloading path (DO) after completion of back transformation as shown in the Fig. 3. The equations are now rewritten as follows:

- If $x_b\dot{x}_b > 0$ (OAB path)

$$\dot{f}_{rs} = k_a\left[\dot{x}_b - |\dot{x}_b|\left(\frac{f_{rs}-\beta}{F_{ys}}\right)^n\right] \tag{19}$$

$$\beta = k_t\left\{x_b - \frac{f_{rs}}{k_a}\right\} \tag{20}$$

- If $x_b\dot{x}_b < 0$ and $x_b > x_{af}$ (BCD path)

$$\dot{f}_{rs} = k_m\left[\dot{x}_b - |\dot{x}_b|\left(\frac{f_{rs}-\beta}{F_{ym}}\right)^{n'}\right] \tag{21}$$

$$\beta = k_m\alpha_s\left\{x_b - \frac{f_{rs}}{k_a} + f'_T|x_b|^{c'}erf\left(a'x_b\right)[u(-x_b\dot{x}_b]\right\} \tag{22}$$

where x_{af} is the displacement when the back transformation completed; k_m is the martensite stiffness; and the yield force F_{ym} is evaluated as

$$F_{ym} = F_{ys}\frac{k_m}{k_a} \tag{23}$$

- If $x_b\dot{x}_b < 0$ and $x_b < x_{af}$ (DO path)

$$\dot{f}_{rs} = k_a\left[\dot{x}_b - |\dot{x}_b|\left(\frac{f_{rs}-\beta}{F_{ys}}\right)^n\right] \tag{24}$$

$$\beta = k_t\left\{x_b - \frac{f_{rs}}{k_a} + f_T|x_b|^{c'}erf\left(a'x_b\right)[u(-x_b\dot{x}_b]\right\} \tag{25}$$

Other unnoted parameters have already been defined. The values of k_a, k_m, k_t and hysteresis constants are taken same as used in Ren et al. [30].

4. Dynamic analysis

The earthquake excitation demands the ductility ratio more than 20 or higher by the isolator [36]. Since the SMA is well known for ductility, the ductility ratio of SMA can be more than 20. Thus, in the present work, the ductility ratio considered for isolator is 20. The seismic response of benchmark base-isolated building is obtained under seven real earthquake ground motions. These earthquake ground motions are given in the benchmark problem as tabulated in Table 2. The mentioned pulse type earthquakes are well known near fault earthquakes. The pulse-type behavior of these earthquake ground motions is conspicuously clear from their displacement, velocity and acceleration spectra presented by Sharma and Jangid [37]. These earthquake ground motions are scaled by the iterating procedure in order to get design displacement of 0.2 m. The scale factors are considered satisfactory when the relative error between computed peak displacement and design displacement is within 1%. The corresponding scale factors are used for analysis with equivalent linear model of SMA. The equivalent linear resultant forces in the SMA wires are computed for 0.2 m design displacement by using proposed equivalent linear elastic-viscous model as illustrated in Section 3.1. The nonlinear and its equivalent linear resultant forces of SMA wires are computed in such a way that, it represents the force-deformation behavior as mentioned in Section 3.2.

The evaluation criteria (EV) given in the benchmark problem is selected for study. These evaluation criteria are reported in the Table 3. The corresponding fixed base structural responses are tabulated in the Table 4. The response quantities are normalized by corresponding fixed base values. The equations of motion of base-isolated building are solved numerically using Newmark's method of step-by-step integration for nonlinear SMA models and its equivalent linear model. The linear variation of acceleration over a small time interval, $\delta t = 0.001$ s is adopted.

5. Comparative study of nonlinear SMA models and its equivalent linear model

A comparative study of nonlinear SMA models with its equivalent linear model for base-isolated benchmark building has been carried out in this section. The normalized response values obtained by dynamic analysis of the base-isolated benchmark building with nonlinear SMA models or its equivalent linear model are tabulated in Table 5.

Table 2
Details of earthquake ground acceleration records.

Serials	Earthquake	Year	Station	Direction	Scale factor
GM1	Northridge	17/01/1994	Newhall	360 as FN	0.65
GM2	Imperial Valley	19/05/1940	El Centro Array	180 as FN	0.99
GM3	Northridge	17/01/1994	Rinaldi	228 as FN	0.46
GM4	Kobe	16/01/1995	JMA	000 as FN	0.69
GM5	Taiwan	10/15/1999	Jiji TCU 068	N as FN	0.21
GM6	Turkey	1/10/1995	Erzincan	NS as FN	0.30
GM7	Northridge	17/01/1994	Sylmar	360 as FN	0.30

Table 3
Evaluation Criteria (EV).

Peak base shear	Peak story shear	Peak base displacement	Peak story drift
$J_1 = \frac{max\|(V_b(t))\|}{max\|(\widehat{V_b}(t))\|}$	$J_2 = \frac{max\|(V_s(t))\|}{max\|(\widehat{V_s}(t))\|}$	$J_3 = \frac{max\|(x_{max}(t))\|}{max\|(\widehat{x_{max}}(t))\|}$	$J_4 = \frac{max\|(d_f(t))\|}{max\|(\widehat{d_f}(t))\|}$
Peak absolute acceleration	Peak cumulative isolation force	RMS base displacement	RMS absolute acceleration
$J_5 = \frac{max\|(a_f(t))\|}{max\|(\widehat{a_f}(t))\|}$	$J_6 = \frac{max\|(F_b(t))\|}{max\|(\widehat{F_b}(t))\|}$	$J_7 = \frac{max\|(RMSx_{max}(t))\|}{max\|(\widehat{RMSx_{max}}(t))\|}$	$J_8 = \frac{max\|(RMSa_f(t))\|}{max\|(\widehat{RMSa_f}(t))\|}$

V_b and V_s = Base and Structural shear; F_b = Isolation force; RMS = Root mean square; $\widehat{\ }$ = Corresponding fixed base response quantity a_f = top-floor acceleration; d_f = Inter story drift; t= Time; $\|.\|$ = Modulus of Vector magnitude.

Table 4
Fixed-base response values.

Serials	Maximum Base Shear (kN)	Maximum Story Shear (kN)	Maximum Base Disp. (m)	Maximum Story Drift (m)	Maximum Absolute Accln. (m/s^2)	Maximum Force (kN)	Maximum RMS Base Disp. (m)	Maximum RMS Absolute Accln. (m/s^2)
GM1	198147	171903	1	0.06	24.12	1	1	3.34
GM2	71313	62546	1	0.02	7.14	1	1	2.11
GM3	244642	231206	1	0.08	27.10	1	1	5.14
GM4	199662	190084	1	0.09	26.24	1	1	5.01
GM5	121324	113733	1	0.04	11.18	1	1	2.22
GM6	112623	105099	1	0.04	11.04	1	1	2.01
GM7	183959	154157	1	0.05	17.27	1	1	2.17

The responses like displacement and isolation force for fixed-base structure are irrelevant, hence the value is considered as unity.

Table 5
Comparison of obtained EV criterion values for base-isolated benchmark building by non-linear models and its proposed equivalent linear model.

EV	Model	Newhall	Elcentro	Rinaldi	Kobe	Jiji	Erzican	Sylmar
J_1	G-C	0.89	0.13	0.32	0.19	0.69	0.65	0.59
	Ren et al.	0.92	0.12	0.33	0.20	0.70	0.66	0.60
	Equivalent Linear	0.93	0.10	0.35	0.22	0.68	0.63	0.63
J_2	G-C	0.79	0.11	0.28	0.15	0.61	0.56	0.58
	Ren et al.	0.82	0.10	0.29	0.16	0.62	0.57	0.59
	Equivalent Linear	0.79	0.08	0.31	0.19	0.61	0.55	0.61
J_3	G-C	0.20	0.20	0.20	0.20	0.20	0.20	0.20
	Ren et al.	0.20	0.20	0.20	0.20	0.20	0.20	0.20
	Equivalent Linear	0.18	0.16	0.18	0.16	0.16	0.18	0.15
J_4	G-C	0.31	0.12	0.08	0.09	0.17	0.17	0.16
	Ren et al.	0.31	0.12	0.09	0.10	0.17	0.18	0.16
	Equivalent Linear	0.40	0.09	0.11	0.13	0.15	0.15	0.14
J_5	G-C	0.37	0.12	0.15	0.13	0.38	0.34	0.32
	Ren et al.	0.38	0.13	0.15	0.13	0.39	0.34	0.33
	Equivalent Linear	0.42	0.11	0.20	0.15	0.35	0.30	0.34
J_6	G-C	0.13	0.13	0.13	0.13	0.12	0.12	0.13
	Ren et al.	0.13	0.13	0.13	0.12	0.13	0.13	0.13
	Equivalent Linear	0.17	0.10	0.16	0.17	0.09	0.08	0.09
J_7	G-C	0.05	0.04	0.05	0.04	0.07	0.05	0.06
	Ren et al.	0.05	0.04	0.05	0.04	0.08	0.05	0.06
	Equivalent Linear	0.02	0.02	0.02	0.02	0.05	0.02	0.02
J_8	G-C	0.29	0.21	0.15	0.13	0.41	0.34	0.42
	Ren et al.	0.30	0.21	0.15	0.14	0.43	0.36	0.44
	Equivalent Linear	0.29	0.16	0.13	0.13	0.32	0.30	0.40

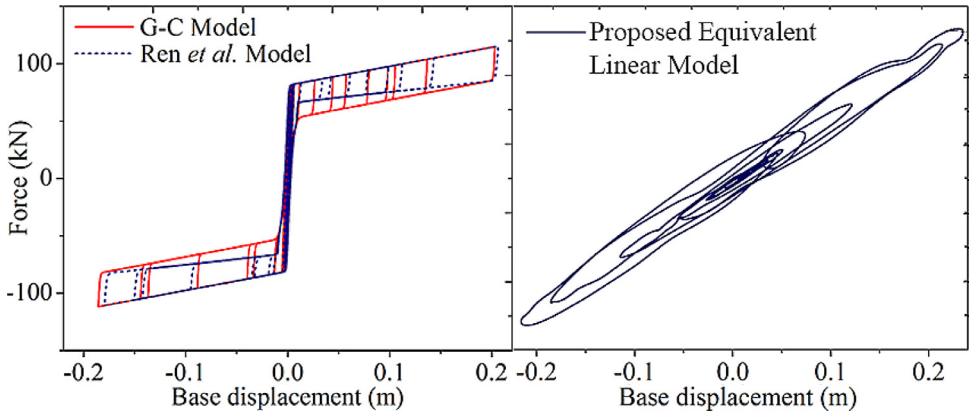

Fig. 4. Force deformation behavior of nonlinear SMA models and its proposed equivalent linear model for Newhall (1994) earthquake.

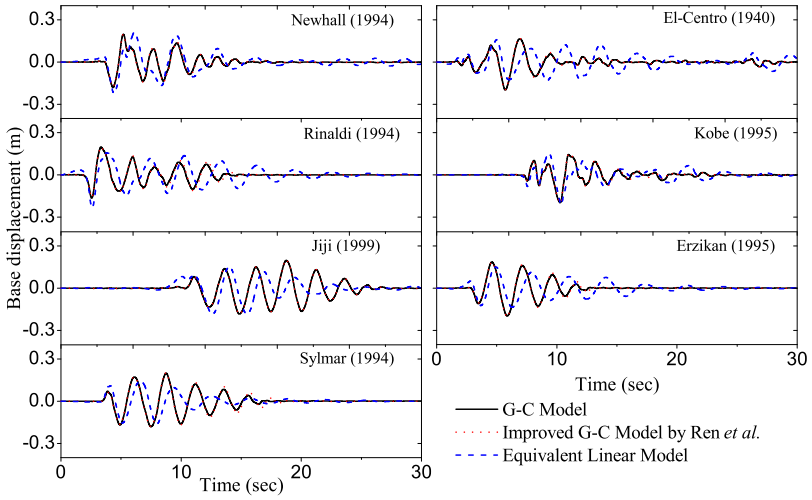

Fig. 5. Time variation of base displacement for base-isolated benchmark building.

In this attempt, $J_3 = 0.20$ and $J_7 = 0.05$ response values are obtained from nonlinear SMA models under Newhall (1994) earthquake. Whereas in the case of proposed equivalent linear model these are 0.18 and 0.02. It implies that equivalent linear model of SMA moderately under estimates the base-displacement response. The same comparison is observed by most of the earthquake ground motions for the base-displacement response. All other responses are moderately over estimated by the equivalent linear model of SMA. The difference between the responses by nonlinear models and its proposed equivalent linear model of SMA is less than 2–5% for all earthquakes excitations.

Fig. 4 depicts the force-deformation behavior of nonlinear classical G-C model, and its extended model by Ren et al. as well as its equivalent linear model. Figures show that the classical G-C model moderately over estimates the hysteretic area within the hysteresis loop than its extended model estimates. It is observed that there is no significant variation in the area of hysteresis loop. However, slight decrease in the slope of unloading path is observed during martensite to austenite transformation. The area of the hysteresis loop (dissipated energy) is marginally reduced by extended G-C model. Hence, reasonably increase in normalized acceleration and base shear responses are obtained by extended G-C model. The force-deformation behavior of proposed equivalent linear model shows the stiffness linearity due to the displacement of base mass and the hysteresis loop shows the viscous damping due to the velocity component of base mass. It can be concluded that both G-C model and G-C's extended model give the same response for larger displacement by neglecting reduction in hysteresis area within the hysteresis loop.

The floor accelerations developed in the superstructure are proportional to the forces exerted in the structure. On the other hand, the bearing displacement is important to limit the isolation device displacement [19]. Thus, the time history variations of top-floor absolute acceleration and base-displacement are considered for the present study. The time variation of base-displacement and top-floor acceleration are depicted in Figs. 5 and 6, respectively. It shows that the peak acceleration responses of nonlinear models and proposed equivalent linear model of SMA are comparable, but more acceleration frequency is induced by the nonlinear model of SMA. Therefore, it can be concluded that the nonlinear SMA models and its proposed equivalent linear model show comparable peak response of the base-isolated benchmark building. The proposed equivalent linear model of SMA is modified form of AASHTO guidelines specifications. Therefore the practicing engineers can freely use it in their design.

6. Conclusions

The response of the base-isolated benchmark building with SMA supplemented ERB isolation systems is carried out by time history analysis. An equivalent elastic-viscous model of SMA is proposed to simulate the nonlinear behavior of SMA. From the present study, following conclusions can be drawn.

1. The effective stiffness of nonlinear SMA model shows similar pattern as that of bilinear model. Therefore, the AASHTO isolation guidelines for bi-linear system can be used for effective stiffness of nonlinear SMA model.

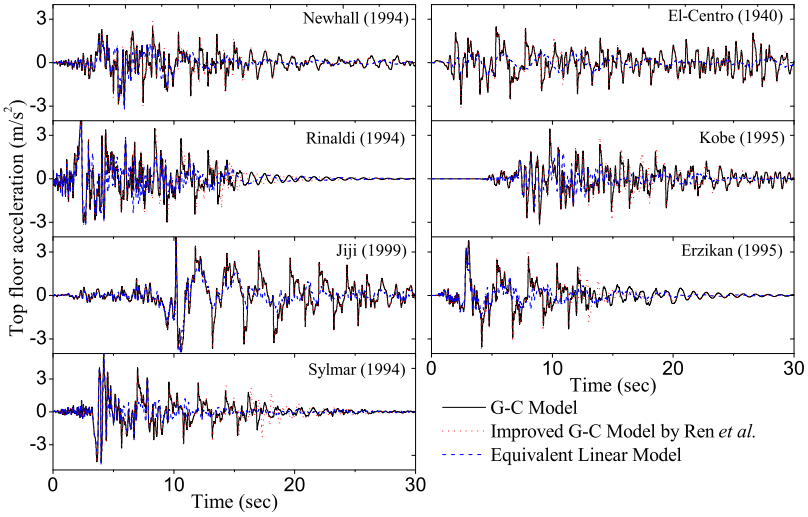

Fig. 6. Time variation of top floor acceleration for base-isolated benchmark building.

2. Nonlinear SMA models and the proposed equivalent linear model shows the comparable peak response of the base isolated benchmark building.
3. As the proposed equivalent linear model is established by using system identification method, this model is valid for any type of isolated structures (i.e. Bridges, Buildings, Water tanks etc.).
4. Both nonlinear G-C and G-C's extended model show almost similar response at larger displacement. This may be attributed to the insignificant difference between the estimated hysteresis area by these two models.
5. The proposed equivalent linear model of SMA is a modified form of AASHTO guidelines specifications, and therefore practicing engineers can freely use it in the design.

References

[1] Chang C-M, Park K-S, Mullenix A, Spencer BF. Semiactive control strategy for a phase II smart base isolated benchmark building. Struct Control Health Monit 2008;15(5):1545–2263.
[2] Sahasrabudhe S, Nagarajaiah S. Sliding isolated buildings with smart dampers: Shaking table studies. Structures 2001 2001;97:1–8.
[3] Narasimhan S, Nagarajaiah S. Smart base isolated buildings with variable friction systems: H∞ controller and SAIVF device. Earthq Eng Struct Dyn 2006;35(8):1096–9845.
[4] Nagarajaiah S, Narasimhan S. Seismic control of smart base isolated buildings with new semiactive variable damper. Earthq Eng Struct Dyn 2007;36(6):729–49.
[5] Choi E, Nam T-h, Cho B-S. A new concept of isolation bearings for highway steel bridges using shape memory alloys. Can J Civil Eng 2005;32(5):957–67.
[6] Dezfuli FH, Alam MS. Shape memory alloy wire-based smart natural rubber bearing. Smart Mater Struct 2013;22(4):045013.
[7] Dezfuli FH, Alam MS. Hysteresis model of shape memory alloy wire-based laminated rubber bearing under compression and unidirectional shear loadings. Smart Mater Struct 2015a;24(6):065022.
[8] Zhang Y, Hu X, Zhu S. Seismic performance of benchmark base-isolated bridges with superelastic cu-al-be restraining damping device. Struct Control Health Monit 2009;16(6):668–85.
[9] Mahjoubi S, Maleki S. Seismic performance assessment of steel frames equipped with a novel passive damper using a new damper performance index. Struct Control Health Monit 2015;22(4):774–97.
[10] Casciati F, Faravelli L, Hamdaoui K. Performance of a base isolator with shape memory alloy bars. Earthq Eng Eng Vib 2007;6(4):401–8.
[11] Casciati S, Faravelli L. Structural components in shape memory alloy for localized energy dissipation. Comput Struct 2008;86(3-5):330–9.
[12] Casciati F, Faravelli L. A passive control device with SMA components: from the prototype to the model. Struct Control Health Monit 2009;16(7-8):751–65.
[13] Attanasi G, Auricchio F, Fenves GL. Feasibility assessment of an innovative isolation bearing system with shape memory alloys. J Earthq Eng 2009;13(1):18–39.
[14] Ozbulut OE, Hurlebaus S. Application of an SMA-based hybrid control device to 20-story nonlinear benchmark building. Earthq Eng Struct Dyn 2012;41(13):1831–43.
[15] Ozbulut OE, Hurlebaus S, Desroches R. Seismic response control using shape memory alloys: a review. J Intell Mater Syst Struct 2011;22(14):1531–49.
[16] International Building Code. 2000. International Code Council.
[17] Uniform Building Code. International Conference of Building Officials, California: Whittier; 1997.
[18] Hwang JS, Chiou JM. An equivalent linear model of lead-rubber seismic isolation bearings. Eng Struct 1996a;18(7):528–36.
[19] Matsagar VA, Jangid RS. Influence of isolator characteristics on the response of base-isolated structures. Eng Struct 2004;26(12):1735–49.
[20] Ghodke SL, Jangid RS. An equivalent elastic-viscous model of shape memory alloy supplemented isolation bearing. In: Topping B, Ivanyi P, editors. Proceedings of the Twelfth International Conference on Computational Structures Technology, Civil-Comp Press, Stirlingshire, UK, Paper 65; 2014.
[21] Narasimhan S, Nagarajaiah S, Johnson EA, Gavin HP. Smart base-isolated benchmark building. part i: problem definition. Struct Control Health Monit 2006;13(2-3):573–88.
[22] Nagarajaiah S, Narasimhan S. Smart base-isolated benchmark building. part II: phase i sample controllers for linear isolation systems. Struct Control Health Monit 2006;13(2-3):589–604.
[23] Erkus B, Johnson EA. Smart base-isolated benchmark building part III: A sample controller for bilinear isolation. Struct Control Health Monit 2006;13(2-3):605–25.
[24] American Association of State Highway and Transportation Officials. Guide specifications for seismic isolation design. Washington, D.C.: American Association of State Highway and Transportation Officials; 1991.
[25] Baratta A, Corbi O. Super-elastic SMA dissipation and re-centering effect in structures subject to dynamic motion. In: Topping B, Ivanyi P, editors. Proceedings of the Twelfth International Conference on Computational Structures Technology, Civil-Comp Press, Stirlingshire, UK, Paper 67; 2014.
[26] Graesser EJ, Cozzarelli FA. Shape-memory alloys as new materials for a seismic isolation. J Eng Mech 1991;117:2590–608.
[27] Feng ZC, Li DZ. Dynamics of a mechanical system with a shape memory alloy bar. J Intell Mater Syst Struct 1996;7(4):399–410.
[28] Wilde K, Gardoni P, Fujino Y. Base isolation system with shape memory alloy device for elevated highway bridges. Eng Struct 2000;22(3):222–9.
[29] Zhang Y, Zhu S. A shape memory alloy-based reusable hysteretic damper for seismic hazard mitigation. Smart Mater Struct 2007;16(5):1603–13.
[30] Ren W, Li H, Song G. A one-dimensional strain-rate-dependent constitutive model for superelastic shape memory alloys. Smart Mater Struct 2007;16(1):191–7.
[31] Ozdemir H. Nonlinear transient dynamic analysis of yielding structures, Berkeley, CA: University of California; 1976. Ph.D. thesis.
[32] Baratta A, Corbi O. On the dynamic behavior of elastic-plastic structures equipped with pseudoelastic SMA reinforcements. Comput Mater Sci 2002;25(1-2):1–13.
[33] Corbi O. Shape memory alloys and their application in structural oscillations attenuation. Simul Model Pract Theory 2003;1(5-6):387–402.
[34] Torra V, Carreras G, Casciati S, Terriault P. On the niti wires in dampers for stayed cables. Smart Struct Syst 2014;13(3):353–74.
[35] Dezfuli FH, Alam MS. Hysteresis model of shape memory alloy wire-based laminated rubber bearing under compression and unidirectional shear loadings. Smart Mater Struct 2015b;24(6):065022.
[36] Hwang JS, Chiou JM. An equivalent linear model of lead-rubber seismic isolation bearings. Eng Struct 1996b;18(7):528–36.
[37] Sharma A, Jangid RS. Seismic response of base-isolated benchmark building with variable sliding isolators. J Earthq Eng 2010;14(7):1063–91.